AIAA JOURNAL
Vol. 47, No. 12, December 2009

Pressure Oscillations from Cavities with Ramp

N. S. Vikramaditya* and Job Kurian†
Indian Institute of Technology Madras, Chennai 600 036, India

DOI: 10.2514/1.43068

Study on supersonic flow over wall-mounted cavities with different ramp angles is carried out experimentally. Experiments include instantaneous shadowgraph visualization and unsteady pressure measurements. In the case of cavities with ramp angles of 90, 75, and 60 degrees, four different types of waves were observed in the supersonic flow above the cavity. The shear layer appeared predominantly wavy in nature. The wave system observed in the case of cavities of 90, 75 and 60 degrees is distinctly different from that in cavities of 45, 30, and 15 degrees. In the case of cavities with higher ramp angles, high-amplitude tones were observed and the presence of an upstream-traveling acoustic wave could be confirmed. A cavity with a ramp angle of 45 degrees was found to reduce the amplitude of oscillations. An increase in amplitude of oscillations at various locations inside the cavity has been observed for cavities with ramp angles of 30 and 15 degrees. This is in contrast to the cavity with a ramp angle of 45 degrees. The reasons for this ambiguous behavior could not be ascertained. The presence of a forward-moving acoustic wave could not be identified in the cavities with ramp angles of 45, 30, and 15 degrees. Temporal mode switching occurring in cavities with higher ramp angles was confirmed by spectrogram studies.

Nomenclature

D	=	depth of the cavity
f	=	frequency, Hz
k_c	=	ratio of speed of convection of shed vortices to freestream speed
L	=	length of the cavity
L/D	=	length-to-depth ratio of the cavity
M_∞	=	freestream Mach number
n	=	mode number
P_{rms}	=	root-mean-square pressure
r	=	recovery factor
U_∞	=	freestream velocity
x	=	distance from the leading edge of the cavity
α	=	time lag in phase relation
γ	=	ratio of specific heat
θ	=	ramp angle with respect to horizontal

I. Introduction

SUPERSONIC flow past rectangular cavities has been studied comprehensively over the years. The applications of such a flowfield are in aircraft weapon bays, wheel wells, in-flight fueling ports, and a host of other situations. It is known from earlier studies that such flows generate self-sustained oscillations that produce high-amplitude tones, thereby causing serious concern about the structure of aerospace vehicles. A good amount of research work, both experimental and numerical, has been undertaken, mainly to understand the physics of the flowfield. It is understood that one of the principal reasons for such a complex flowfield is the presence of a subsonic recirculation zone inside the cavity. There are several parameters on which the structure of the flowfield depends: a few among them are the nature of the approaching boundary layer, Mach number of the flow, and length/depth ratio L/D of the cavity. Krishnamurthy [1] was the first to identify the oscillatory behavior of the cavity flowfield for a wide range of supersonic Mach numbers. Rossiter [2] proposed an empirical formula and explained the origin of self-sustained oscillations for flow ranging from low-subsonic to transonic Mach numbers. Heller et al. [3] modified the Rosssiter formula suitably to take supersonic flows into account. Rockwell and Naudascher [4] described the oscillations as basically of two types: 1) fluid-dynamic and 2) fluid-resonant. It was proposed that purely fluid-dynamic oscillations occur if the ratio of cavity length to acoustic wavelength is very small, and purely resonant oscillation occurs if the corresponding wavelength of the acoustic wave is of the same order of magnitude as the characteristic length of the cavity. Zhang and Edwards [5] observed that if the cavity L/D ratio is less than or equal to unity, the oscillations are transverse in nature, whereas for L/D greater than 2, the oscillations are longitudinal. Several control techniques [6–14], both passive and active, have been employed to control the oscillations. A few such devices implemented successfully are static and oscillating fences, steady and pulsating flow injection, flowpath modifiers at the bottom of the cavity, and slanted trailing walls. Zhang et al. [15] showed that open cavities with very small aft-wall angles lead to steady shear-layer reattachment. The slanted trailing edge modifies the shear-layer reattachment process such that pressure waves are not sent back into the cavity. Kuo and Huang [16] investigated the effect of sloped bottom and flowpath modifier at the bottom of the cavity on cavity oscillation in a recirculating water channel. It was observed by them that a negatively sloped bottom has the ability to suppress the self-excited oscillations of cavities. Perng and Dolling [17], in their experimental study, evaluated the effectiveness of various modifications such as slotted, vented, slant, beak, and valley aft walls in suppressing the pressure oscillations generated by high-Mach-number flows over the cavity. Gruber et al. [18] experimentally and computationally studied the flowfield over cavities with different aft-wall angles and offset ratios. Their study involved flow visualization and static pressure measurement in the vicinity of the cavity to identify potential configuration for flame holding. The study was limited to rectangular cavities with low aft-wall angles of 30 and 16 deg. Sun et al. [19] observed that as the cavity L/D of the cavity decreases, oscillation frequency corresponding to maximum oscillation amplitude shifts to higher values. The modes of oscillation are greatly suppressed as the cavity aft-wall angle decreases. In contrast to the steep aft-wall cavity, only higher-frequency modes of oscillation remain in the case of the cavity with a small aft-wall angle.

The aim of the present study is to understand the behavior of cavities with different ramp angles based on the characteristics of oscillations they produce when a supersonic flow passes over the cavity. It further tries to understand the influence of ramp angle on the oscillatory behavior of the cavity. Based on the present studies, an

Received 16 January 2009; revision received 20 July 2009; accepted for publication 3 August 2009.

*Ph.D. Student, Department of Aerospace Engineering; vikram_sri@yahoo.com.

†Professor, Department of Aerospace Engineering; kurian@ae.iitm.ac.in.

attempt is made to understand the physics of the flow with a change in the geometry of the cavity.

II. Experimental Details

All of the experiments were performed in the supersonic free-jet facility at the Indian Institute of Technology Madras. This facility is supplied with compressed air from three external reservoirs with a total capacity of 36 m^3 and a maximum stagnation pressure of 13.4 bar absolute. An 8-in.-diam pipeline connects the external reservoirs with the settling chamber of the free-jet facility. The stagnation pressure of the flow is maintained at 5.4 bar absolute, and the stagnation temperature is the ambient temperature in the present experiments. The outlet of the settling chamber is connected with a circular-to-rectangular transition duct. A nozzle is attached to the rectangular end of the transition duct.

The nozzle is calibrated using the total and static pressure readings taken across the exit area. The estimated error in the pressure measurements is found to be less than $\pm 1\%$. The calibrated Mach number obtained at the exit of the nozzle is 1.63. The 280-mm-long rectangular test section is of 30 mm height and 57 mm width. The test section is made of Perspex. The cavity was accommodated along the bottom wall of the test section, 80 mm downstream of the nozzle exit. Figure 1 shows the schematic of the test section along with the cavity.

Six cavity models were made with a constant L/D ratio of 3, as shown in Fig. 2, and with different ramp angles θ. Holes were drilled along the center plane of the aluminum models to locate pressure transducers at selected locations for the measurements of fluctuating pressure. The cavity dimensions tested in the present study are summarized in Table 1.

The length of the angled cavity is defined as the distance from the leading edge to the midchord of the cavity back face, and the effective length of the cavity is defined as the distance from the leading edge to the trailing edge. The length and depth of the cavity models are constant and equal to 60 and 20 mm, respectively. The width of the cavity ($W = 57$ mm) spans the entire test section. The height $D1$ is 10 mm, which is constant for all cavity models under study.

The boundary layer is taken to grow from the nozzle throat, and the Reynolds number of the boundary layer approaching the cavity leading edge is calculated to be 7.46e + 07/m. The incoming test-section floor boundary layer undergoes natural transition far upstream of the cavity leading edge and becomes turbulent well ahead of the cavity under approximately adiabatic-wall temperature conditions. Laser Doppler velocimetry (LDV) is used to measure freestream velocity and the boundary-layer thickness 1 mm ahead of the cavity leading edge. The freestream velocity inside the test section is 484 m/s, and the thickness of the boundary layer is 6 mm. The level of freestream turbulence is 0.62%. The two-dimensionality of the flowfield is confirmed by LDV measurements, which have shown that variation of freestream velocity at various spanwise locations is less than $\pm 1\%$ up to a distance of 20 mm on both sides of the center plane.

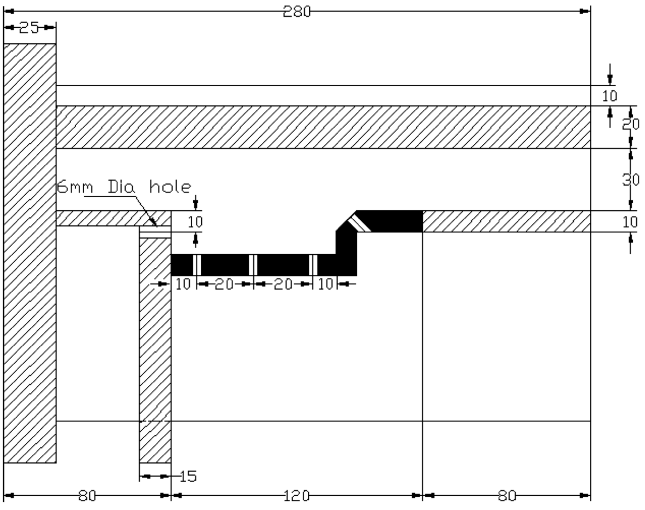

Fig. 1 Schematic of test section containing the cavity with a ramp.

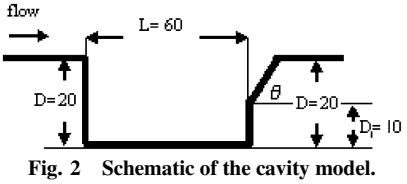

Fig. 2 Schematic of the cavity model.

Table 1 Cavity dimensions

Model no.	Effective length, mm	Ramp angle, deg
1	60	90
2	62.68	75
3	65.77	60
4	70	45
5	77.32	30
6	97.32	15

Instantaneous shadowgraph technique was used to observe the flowfields in the vicinity of the cavities. For the instantaneous imaging, a strobe light that gives a spark for about 18 ns duration is used as the source of illumination and is found to be sufficient to capture most of the flow features. The instantaneous images are acquired with a high-speed digital complementary metal-oxide semiconductor camera HS-3 model manufactured by Redlake, USA. The strobe light is synchronized with the high-speed camera.

Piezoelectric pressure transducers (PCB Piezotronics, model no. 112A22) are used to perform the fluctuating pressure measurements. These transducers are flush-mounted on the cavity surface. The transducer signal is passed through a signal conditioner and fed to a computer through a 12-bit analog-to-digital data acquisition card (National Instruments PCI-6024E) with a maximum sampling rate of 200 kHz. The signals from the transducers are sampled at 100 kHz for 0.5 s, giving 50,000 samples of unsteady pressure data. These samples are then passed through a low-pass digital filter with a cutoff frequency of 20 kHz. The dominant frequency measured lies within the 0 to 20 kHz range for most of the cavity configurations. In any experiment, only two transducers have been used to acquire signals. Multiple experimental runs with identical flow conditions have been carried out to acquire signals from different transducer locations. The time delay between the signals is 5 μs.

Standard methods of statistical analysis have been used to obtain various quantities of interest. The power spectral densities were computed by segmenting each data record into 25 segments containing 2048 points each, with a transform length of 4096 points. A Hamming window with 50% overlap is used for averaging to get reliable estimate of spectra. The frequency resolution obtained after performing fast Fourier transform (FFT) on each segment is 24.41 Hz. The output of the FFT is used to determine the amplitude of the dominant frequency and its amplitude. All of the experimental test runs are repeated three times. Under identical experimental run conditions, the variations in the dominant frequencies during the repeated tests are within 15 Hz in the 0 to 15 kHz range and those in the amplitudes of the dominant frequencies are 3%. The experimental uncertainty in measuring power spectral densities is equivalent to ± 6 dB. This is obtained by ensemble average of about 25 data sets with 2048 points each.

III. Results and Discussion

A. Flow Visualization

In this section, the flow features of cavities with different ramp angles obtained from instantaneous shadowgraph visualization are presented and discussed. Figure 3 shows the instantaneous shadowgraph images of cavities with different ramp angles. The flow

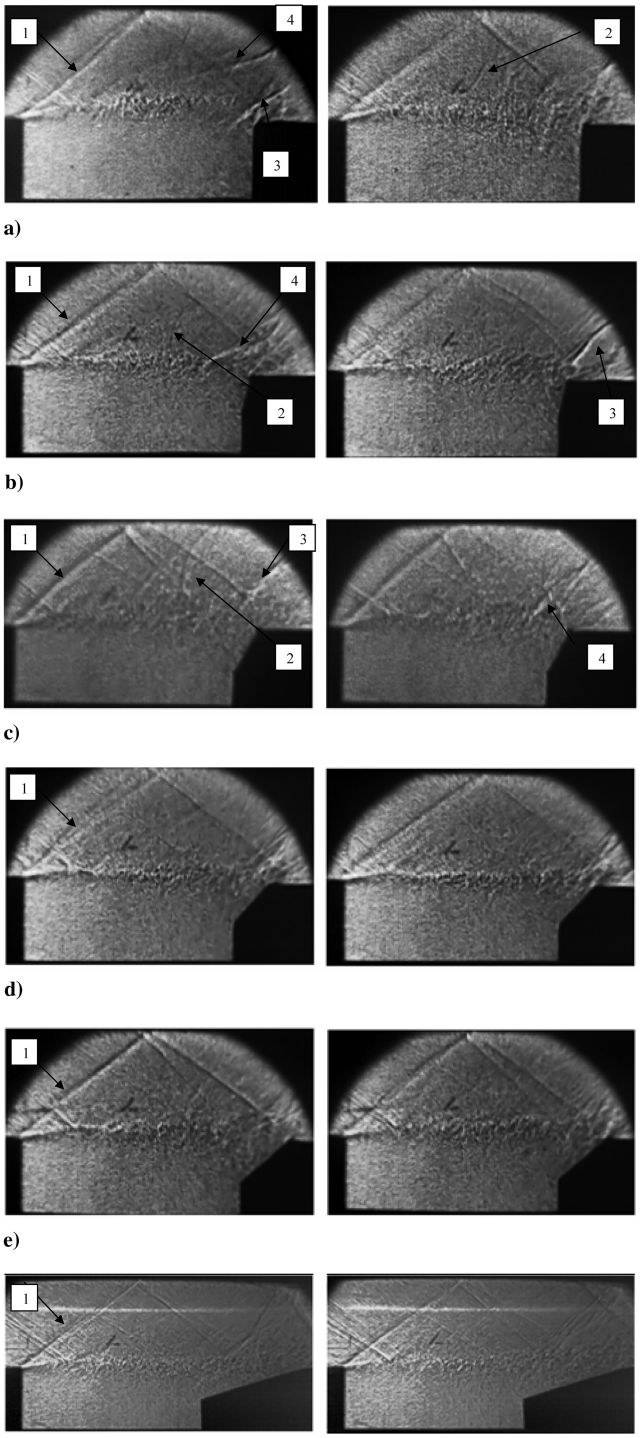

Fig. 3 Instantaneous shadowgraph images of the cavity with ramp angles of a) 90 deg, b) 75 deg, c) 60 deg, d) 45 deg, e) 30 deg, and f) 15 deg.

direction is from left to right. For each cavity, two instantaneous shadowgraph images are presented that represent all the possible flow features observed during one cycle of cavity oscillations. The important feature observed in the images is the existence of large vortices in the shear layer. The vortices are produced by the shear-layer instability, which produces flapping motion, leading to mass entrainment and ejection at the trailing edge of the cavity. The shear layer thus experiences a coupled motion of flapping in the transverse direction and vortex convection in the streamwise direction. It is observed that the flapping motion of the shear layer reduces with the decrease in the ramp angle. The unsteady wave motion above the cavity highlights this mechanism.

Figure 3a shows the flow visualization images of the cavity with a ramp angle of 90 deg. Four different waves are observed from the images, as discussed below. As the shear layer "flaps" up and down, it generates a type 1 wave, such as the one indicated in Fig. 3a. It is a compression wave when the shear layer flaps up and is an expansion wave when the shear layer flaps down. Large vortices are visible in the shear layer over the cavity, as noted earlier. A type 2 wave is associated with the convection of vortices in the shear layer. This wave appears very faint in the images. Type 3 is the bow shock observed at the trailing wall of the cavity. This is due to the interaction of supersonic flow with the trailing edge when the shear layer dives into the cavity at the trailing wall. Type 4 is the wave generated due to motion of the acoustic wave inside the cavity. This wave is an imprint of the acoustic wave in the supersonic flow and trails the acoustic wave in the cavity through deflection of the shear layer and moves upstream. The waves similar to those described above were also reported by Zhuang et al. [8]. The presence of waves like the ones observed in the cavity with aft-wall angle of 90 deg were observed in the shadowgraph images of cavities with ramp angles of 75 and 60 deg, as indicated in Figs. 3b and 3c. The shear layer appears extremely wavy in nature, indicating that these cavity flows undergo strong oscillations.

Figures 3d–3f show the shadowgraph images of cavities with ramp angles of 45, 30, and 15 deg. The images indicate the presence of a type 1 wave. The images also indicate the absence of waves marked as types 2–4, which were present in the case of cavities with higher ramp angles. The shear layer is less wavy than that observed in the earlier cavities, suggesting that these cavities are more stable.

The shadowgraph pictures serve to understand the possible effects of the wave reflections in the pressure signals obtained at various locations inside the cavity. The photographs show that the waves generated at the leading edge of the cavity get reflected at the ceiling of the test section. In the case of cavities with ramp angles of 90 to 45 deg, the leading-edge wave did not reflect into the cavity. The leading-edge wave did reflect onto the cavity aft wall in the case of cavities with ramp angles of 30 and 15 deg, as the effective length of the cavity is increased due to the change in ramp angle. However, these reflections did not have any effect on the pressure signals from the transducers in the floor and in the fore wall of the cavities. Further discussion on this is included in the analysis of the pressure signals of 30 and 15 deg ramp cavities in the later part of this paper.

B. Measurement of Unsteady Pressure

In Sec. III.B.1, the experimental results are discussed pertaining to the cavity with a 90 deg aft-wall angle. This is referred to as the baseline case. In the subsequent sections, results related to cavities with 75, 60, 45, 30, and 15 deg ramp angles are presented and discussed. The results from various cavities with different ramp angles are compared in a few cases. Transducer A1 on the front wall is located at 10 mm below the cavity leading edge, and transducer A5 lies 5 mm below the aft wall for the cavity configurations considered for the study.

1. Baseline Cavity

Power spectra in the form of sound pressure level (SPL) vs frequency for transducers positioned at different locations inside the cavity are shown in Fig. 4. Spectra from various locations inside the cavity have been plotted to compare their unsteadiness with respect to each other. The plots are identified as those due to transducer at various x/L locations. The occurrence of discrete large-magnitude peaks corresponding to different cavity tones along with broadband fluctuations can be clearly seen. The multiple peaks at different frequencies are often referred to as different modes of the cavity.

One clear observation from the plot is that, irrespective of the location of the transducer, corresponding cavity tones occur at the same frequency, indicating global instability of the cavity flowfield. Comparison of power spectra at different locations shows that the SPL, in general, increases as one moves from the leading edge to the trailing edge of the cavity. At higher frequencies the spectra becomes broadband (or the spectral peaks become less distinct),

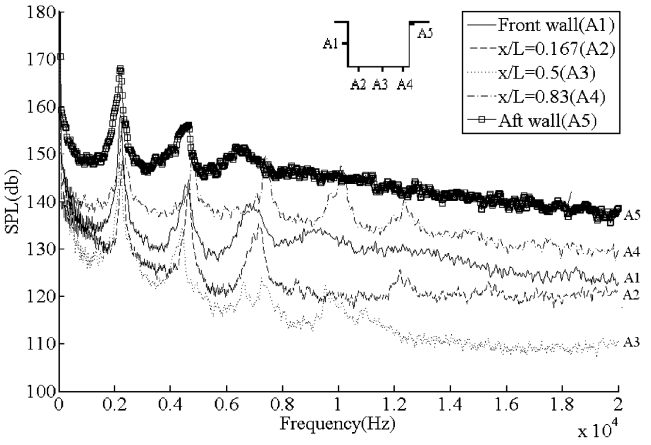

Fig. 4 SPL at different locations inside the baseline cavity.

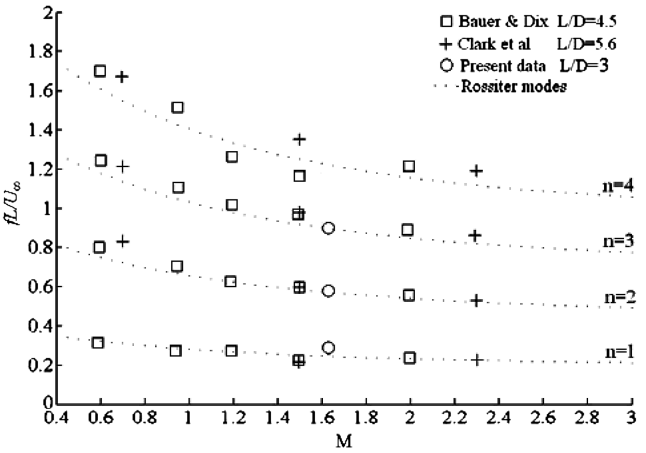

Fig. 5 Variation of Strouhal number with Mach number (Bauer and Dix [20] and Clark et al. [21]).

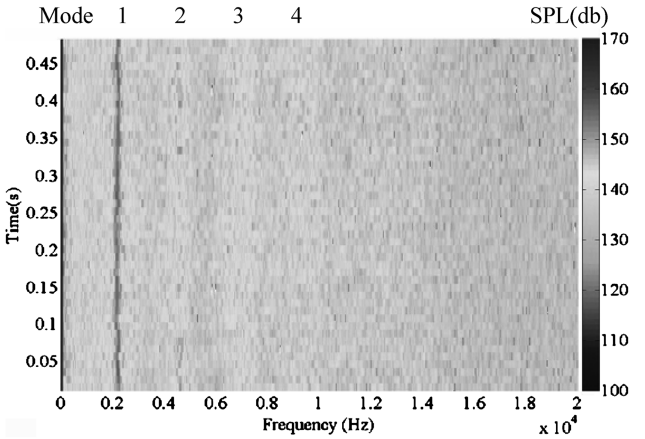

Fig. 6 Spectrogram of the front-wall pressure signal for the baseline cavity.

independently of the location of the transducer. On examining the spectra at different locations individually, it is seen that highest amplitude of modes as well as high-intensity broadband noise are occurring at the aft wall. The high-amplitude peaks occur due to the impingement of the turbulent shear layer and also to the intermittent impingement of shock at the edge of the aft wall. The occurrence of high-amplitude broadband noise is due to the interaction of large structures in the shear layer with the trailing-edge shock. From the leading edge to the trailing edge of the cavity, the turbulent structures in the shear layer grow in size. On observing the front-wall spectra it is seen that the large-amplitude peaks of magnitude equivalent to that of the aft wall exist, but the major difference lies in the broadband noise, which is much less than that of the aft wall. This is justifiable because the shear layer is very thin in the upstream portion of the cavity and the major source of disturbance in this region is the acoustic wave. When comparison is made between transducers flush-mounted on the floor of the cavity, that situated close to the aft wall experiences higher SPL. This is due to the fact that during each cycle of feedback loop there will be entrainment of shear-layer-containing large structures into the cavity. The transducer located at the center of the cavity floor has the lowest level of SPL.

The mode frequencies obtained through experiment are compared with those calculated using Rossiter's modified formula. Rossiter's modified formula is given as follows:

$$\frac{fL}{U_\infty} = \frac{(n-\alpha)}{[M_\infty/\sqrt{1+(r/2)(\gamma-1)M_\infty^2}]+(1/k_c)} \qquad n = 1,2,3,\ldots \tag{1}$$

The value of r is taken as 1 in the present calculation, since the error involved in assuming that the cavity temperature is the freestream stagnation temperature is negligible at lower Mach numbers. Figure 5 presents variation of Strouhal number with Mach number ranging from low subsonic to supersonic. The present data are plotted along with subsonic and supersonic data of Bauer and Dix [20] and of Clark et al. [21]. There is good agreement between the different sets of data and the Rossiter modes. The slight offset in data for other researchers in comparison with Rossiter modes is due to the fact that values of α and k_c are different from those used by Rossiter [2]. This shows that theory of feedback loop proposed by Rossiter is applicable in the present case.

From the SPL vs frequency plot, it is observed how the acoustic energy is distributed among different frequencies. There is no definiteness as to whether all the modes do exist at all times or if shifting of mode from one to the other occurs. To understand this, a short-time Fourier transform was performed on the pressure signals acquired from the front wall. The spectrogram of pressure signal taken from the front-wall transducer is presented in Fig. 6. It shows different modes that are present along with corresponding frequencies and their SPL. On examining the spectrogram, it is noted that the four modes exist and that the first mode is dominating during the entire time for which the signal is acquired. The second mode exists during the initial and final stages of signal acquisition and intermittently during the rest of the times. The occurrence of the third mode is randomly spread over the time period, whereas the fourth mode is almost dormant.

Since multiple transducers were placed at different locations inside the cavity, the output from which are simultaneously sampled, calculation of cross correlation is possible. Figure 7 shows normalized cross-correlation coefficients plotted against time lags for the aft-wall transducer correlated with itself, with two transducers along the floor and with one in the front wall of the baseline cavity. The plots have been curtailed to study a small time separation of the first acoustic wave traveling upstream. The long-time behavior of the curves indicates decaying oscillations. Examining the cross correlation between the front wall and trailing wall, it is seen that when autocorrelation coefficient is maximum, the cross-correlation coefficient is minimum, and vice versa, which suggests that the wave generated at the trailing wall and the wave reflected from the front wall are out of phase by 180 deg. The maximum cross-correlation coefficient is 0.64, corresponding to a time lag of 0.00018 s. This is the time taken by the wave to travel between the aft wall and the front wall. Based on this, one can estimate the speed of the wave inside the cavity. The speed of disturbance calculated was roughly the same as the speed of the acoustic wave traveling between the aft and front walls by considering fluid in the cavity to be stagnant. This is based on the consideration that for low-supersonic Mach numbers, the temperature of fluid inside cavity is the same as the freestream stagnation temperature. The amplitudes of correlation coefficients on the floor of the cavity are 0.34 and 0.43, respectively, in the upstream direction, which are less correlated than those of the front wall. This

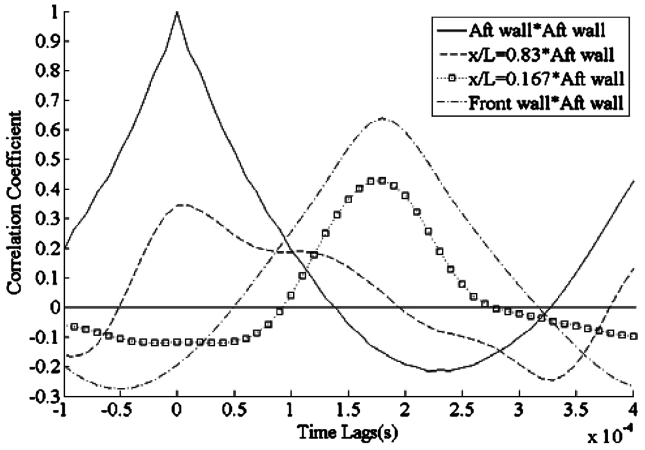

Fig. 7 Normalized cross correlation of pressure signals for the baseline cavity.

indicates that peaks in the correlation function at these locations are not due to a traveling wave front, but could be due to vortex structures inside the cavity.

To understand the relation between different modes occurring at different locations inside the cavity, coherence of pressure signals acquired from the front and aft walls was plotted as shown in Fig. 8. On observing the plot it is noted that there exist three different frequencies at which the value of coherence is very high and one frequency at which the value of coherence is reasonably good. For the other frequencies, the value of coherence is very poor. If Fig. 8 is compared with Fig. 4, it is seen that the frequencies at which the coherence has very high value are the same as those frequencies where distinct peaks or the Rossiter modes exist. This shows that the pressure signals between the front and aft walls at these frequencies are very well correlated.

From this, it can be concluded that the phenomenon responsible for creation of acoustic modes at one location is also responsible for generation of similar kinds of modes at the other location. It is known from the above discussion that high-amplitude tones are due to the presence of an acoustic wave, which is responsible for the feedback mechanism. A high value of coherence between signals at frequencies corresponding to different modes is also a consequence of the same phenomena. This further supports the earlier statement that distinct modes are due to global instability of cavity flow, whereas broadband noise (which has no correlation or poor correlation) is due to turbulent nature of the supersonic flowfield.

2. *Cavity with 75-Degree Ramp Angle*

Spectra in the form of SPL vs frequency for transducers positioned at different locations inside the cavity with a ramp angle of 75 deg are shown in Fig. 9. The qualitative features of the acoustic spectrum of this cavity are the same as that of the 90 deg cavity, though they are marginally different quantitatively. For the 75 deg cavity, the first mode is the dominant one at all the transducer locations. This cavity also exhibits features of global instability similar to the baseline cavity. The highest amplitudes occur at the aft-wall location followed by those at the front wall, as anticipated from the cavity flow behavior. Higher amplitudes occur at the front wall compared with $x/L = 0.83$, whereas broadband noise is higher in $x/L = 0.83$ compared with the front wall. This could be due to incursions of shear layer into the cavity near the aft wall. Although overall spectral features at different transducer locations are very much similar, the amplitudes of modes and their existence at different locations are not similar, because different flow mechanisms come into play from the cavity leading edge to the trailing edge. The behavior of this cavity is almost identical to the baseline cavity.

Figure 10 shows the spectrogram of the front-wall pressure signal. It is seen that four modes occur, of which the first mode is the dominant and exists throughout the time interval for which the signal is acquired. It is also observed that the second and third modes are occurring intermittently. It is also seen that when the second mode dominates, the third mode is absent and weak, and vice versa, respectively. It can be seen that there exists switching from one mode to the other. Unlike the baseline cavity, even though the first mode is dominant for the entire time duration, it can be noted that there exist a good number of time periods in which switching of modes between second and third modes occurs. In the case of the present cavity it can be said that the acoustic energy is rather more distributed over the three modes, unlike the baseline cavity, where most of the energy lies

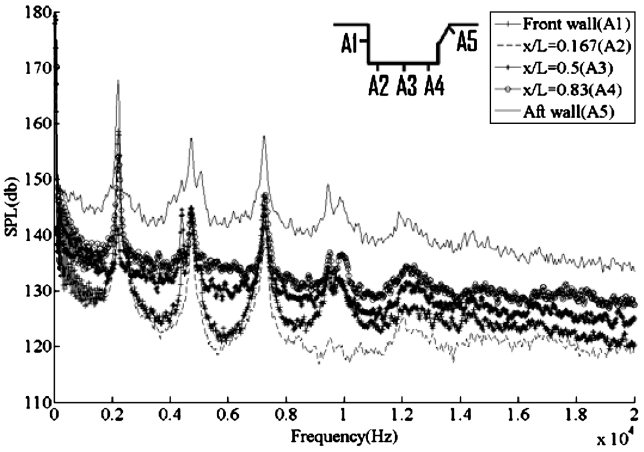

Fig. 9 SPL at different locations inside the cavity with a ramp angle of 75 deg.

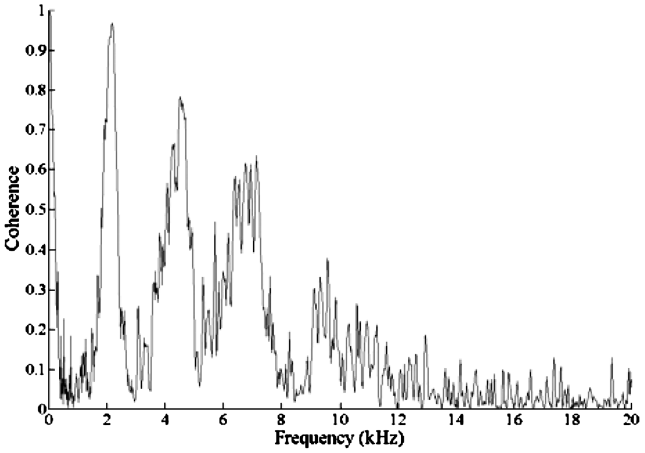

Fig. 8 Coherence between front- and aft-wall pressure signals for the baseline cavity.

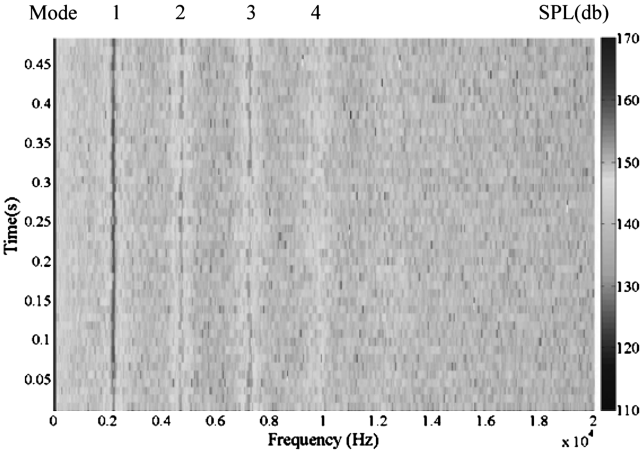

Fig. 10 Spectrogram of the front-wall pressure signal for the cavity with a ramp angle of 75 deg.

with the dominant mode. This shows that the change in ramp angle has a profound effect on acoustic energy distribution. This also implies that oscillations tend to occur in multiple modes rather than in a single mode. The fourth mode is dormant over the entire time duration.

Figure 11 shows the normalized cross-correlation coefficients between the aft wall and different locations inside the cavity. Similar to the baseline cavity, long-time behavior of the curves indicates decaying oscillations. Examining the cross correlation between the front and trailing walls, it is seen that when autocorrelation coefficient is maximum, the cross-correlation coefficient is minimum, and vice versa, which suggests that the wave generated at the trailing wall and the wave reflected from the front wall are out of phase by 180 deg. As in the case of the baseline cavity, this indicates that there exists a standing wave inside the cavity. On observing the cross correlation between the front and aft walls, it is seen that the peak value of cross correlation from the plot is 0.61, which occurs at 0.00018 s. This indicates the existence of the forward-traveling acoustic wave between the aft and front walls in the present cavity case also.

The values of correlation coefficient between $x/L = 0.83, 0.5,$ and 0.167 and the aft wall are 0.4, 0.28, and 0.19, respectively. It can be concluded that in the case of the cavity with a ramp angle of 75 deg, the oscillations are due to the presence of the forward-traveling acoustic wave, as in the baseline cavity.

Coherence between pressure signals acquired from the front and aft walls for the cavity with a ramp angle of 75 deg is shown in Fig. 12. Similar to the baseline cavity, the value of coherence is very high at those frequencies where the modes exist irrespective of amplitude of the modes. For other frequencies, where no modes exist, the value of coherence is very low.

3. Cavity with 60-Degree Ramp Angle

Figure 13 shows the SPL of the pressure signal obtained from different locations inside the cavity with a 60 deg ramp angle. Based on the spectra of the oscillations obtained from the 60 deg cavity, it is seen that the general features are the same as those in the cavities discussed in the previous sections. It is observed that there is a slight drop in amplitudes of the modes at all locations when compared with cavities with higher ramp angles. This is due to the reduction in strength of the acoustic wave due to the change in ramp angle, but the amplitude of the dominant mode is more or less the same.

From Fig. 14, which shows the spectrogram of the front-wall pressure signal, it is observed that the third mode is the dominant one and occurs for the entire time duration for which the signal is captured. The pattern of the other modes in the spectrogram shows that the ramp angle influences mode switching among the different modes.

Figure 15 shows normalized cross correlation between the aft-wall pressure signal and pressure signals from other locations inside the cavity. In the case of the autocorrelation, the maximum correlation coefficient occurs at zero time delay. For other time delays, the magnitude of correlation coefficient is small, indicating that the oscillations have dampened considerably. It is observed that a secondary peak in autocorrelation coefficient and the time lag of this peak correspond to the second Rossiter mode. From Fig. 15, the cross correlation between pressure signals at the front and aft walls has the maximum positive value of 0.43, occurring at time 0.00018 s. This

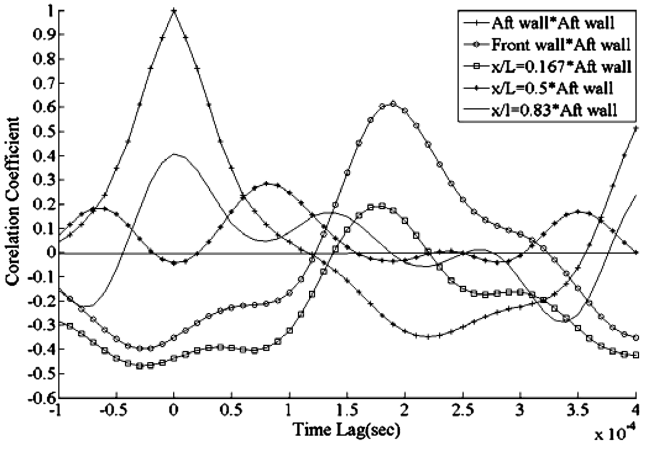

Fig. 11 Normalized cross correlation of pressure signals for the cavity with a ramp angle of 75 deg.

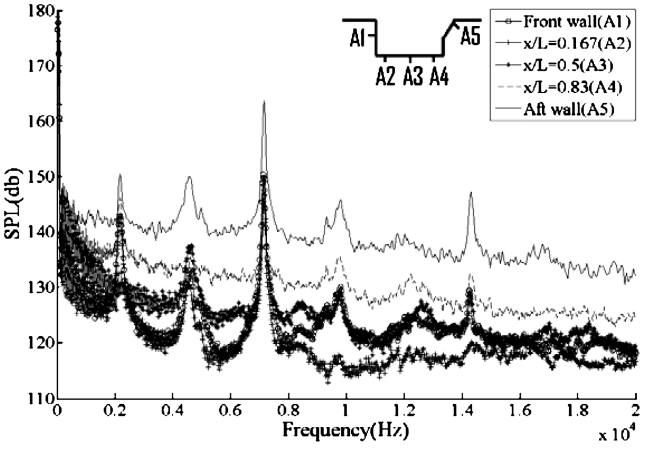

Fig. 13 SPL at different locations inside the cavity with a ramp angle of 60 deg.

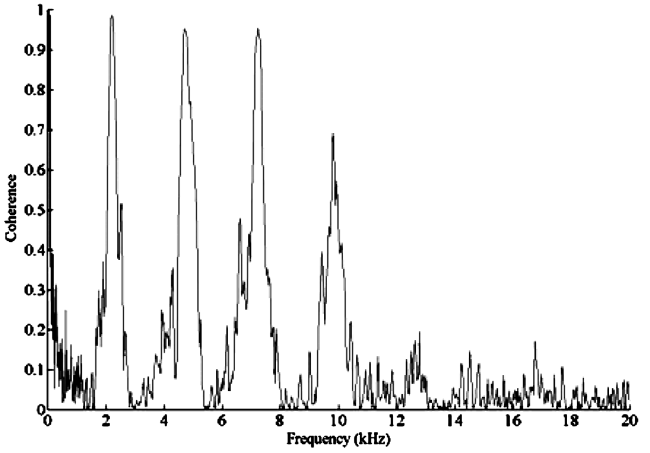

Fig. 12 Coherence between front- and aft-wall pressure signals for the cavity with a ramp angle of 75 deg.

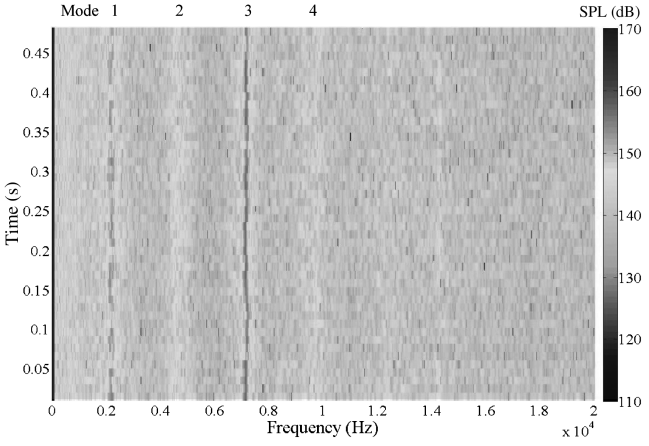

Fig. 14 Spectrogram of the front-wall pressure signal for the cavity with a ramp angle of 60 deg.

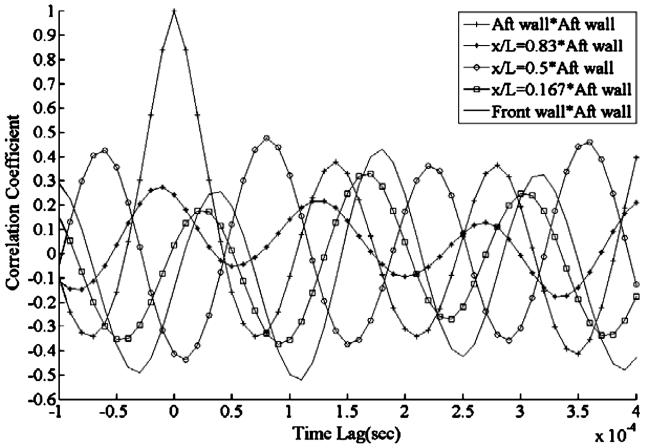

Fig. 15 Normalized cross correlation of pressure signals for the cavity with a ramp angle of 60 deg.

indicates that the forward-traveling acoustic wave does exist in the present cavity case like the higher-ramp-angled cavities. The amplitudes of correlation coefficients on the floor of the cavity at $x/L = 0.167$, 0.5, and 0.83 are 0.33, 0.47, and 0.22, respectively.

Coherence between the front-wall and aft-wall pressure signals is shown in Fig. 16. It is seen that the value of coherence is similar to the baseline cavity and the cavity with a ramp angle of 75 deg. Similar to higher-angled cavities, the value of coherence is very high at those frequencies where the modes exist.

4. Cavity with 45-Degree Ramp Angle

Figure 17 shows the SPL of the pressure signal obtained from different locations inside the cavity with a 45 deg ramp angle. It is observed that there is a steep fall in amplitude of the modes at all locations when compared with cavities with higher ramp angles. The overall broadband noise remains more or less the same.

A spectrogram of the front-wall pressure signal is shown in Fig. 18. It can be seen that five modes exist and that the first and third modes occur rarely, whereas the other modes are almost dormant.

Figure 19 shows normalized cross correlation between the aft-wall pressure signal and pressure signals from other locations inside the cavity plotted for the entire time duration for which signals were acquired. As in the case of the cavities discussed so far, the maximum correlation coefficient occurs at zero time delay, and for other time delays, the magnitude of correlation coefficient is small, indicating that the oscillations have dampened considerably. On observing the cross correlation at different locations except at $x/L = 0.83$, it is observed that at zero time delay, the coefficients have large negative value. This indicates that signals are inversely correlated, which implies that if pressure increases at the trailing wall, there is a decrease in pressure at the other location and vice versa. It is seen that after a large time lag there exists positive correlation between pressure signal from the aft wall and other locations, which is in sharp contrast to cavities with higher ramp angles. Maximum positive cross correlation between pressure signals at the front and aft walls is 0.15, occurring at time 0.38 s. This shows that upstream-traveling disturbance takes a longer time to reach the front wall. One reasonable conclusion could be that unlike in higher-aft-wall-angled

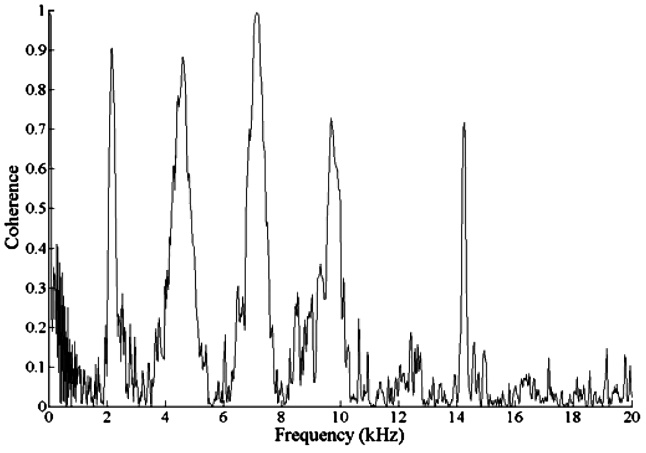

Fig. 16 Coherence between front- and aft-wall pressure signals for the cavity with a ramp angle of 60 deg.

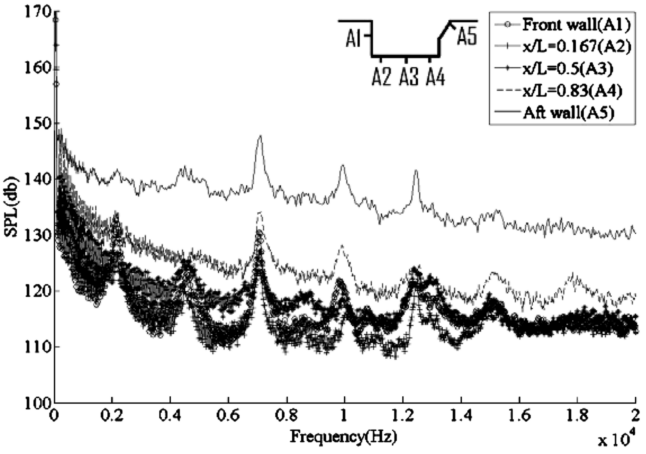

Fig. 17 SPL at different locations inside the cavity with a ramp angle of 45 deg.

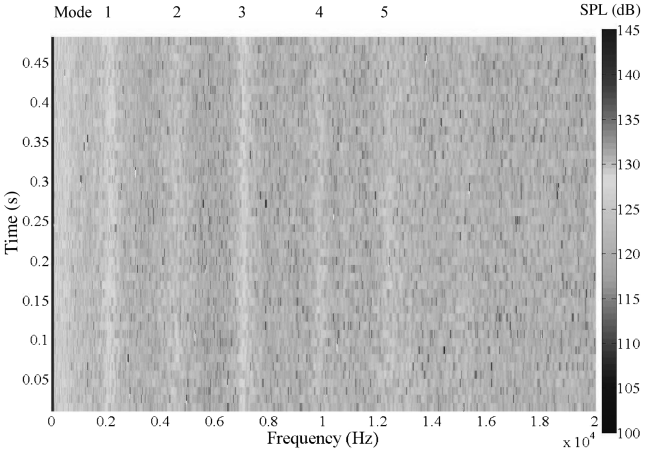

Fig. 18 Spectrogram of the front-wall pressure signal for the cavity with a ramp angle of 45 deg.

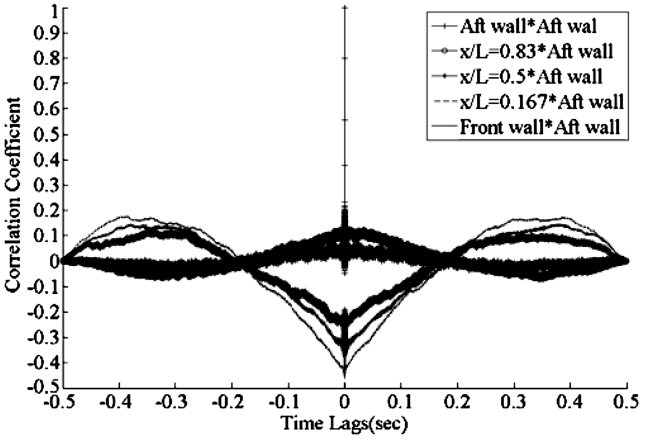

Fig. 19 Normalized cross correlation of pressure signals for the cavity with a ramp angle of 45 deg.

cavities, this disturbance is not an upstream-traveling acoustic wave but a disturbance of some other sort. From this, it can be inferred that the feedback mechanism responsible for the origin of self-sustaining oscillations in higher-aft-wall-angled cavities has substantially weakened in the case of the cavity with a 45 deg aft-wall angle.

Coherence between the front-wall and aft-wall pressure signals is shown in Fig. 20. It is seen that the value of coherence is less in the present case compared with cavities with higher ramp angles at the corresponding mode frequencies. As there is no upstream-traveling wave, the value of coherence is reduced. As mentioned earlier, one of the prime causes of the feedback mechanism for sustaining the oscillations is the acoustic wave. This further substantiates that the feedback-loop mechanism has been attenuated in the case of the cavity with a 45 deg ramp angle.

5. *Cavity with 30- and 15-Degree Ramp Angles*

Figures 21 and 22 show the SPL of pressure signals obtained from different locations inside the cavity with 30 and 15 deg ramp angles, respectively. Considering Fig. 21, it is noted that there is a sudden increase in amplitude of modes with respect to the cavity with a ramp angle of 45 deg. On observing the spectra of the aft-wall signal, it is seen that two distinct modes exist; the magnitude of one mode resembles that of cavities with a ramp angle greater than 45 deg, and the other mode resembles that of the cavity with a 45 deg ramp angle. On examining Fig. 22, a drop in amplitude of modes at the aft-wall location and increase in amplitude of modes at other locations with respect to the cavity with a ramp angle of 30 deg (as seen in Fig. 21) are observed. On observing the spectra of the aft-wall signal, it is seen

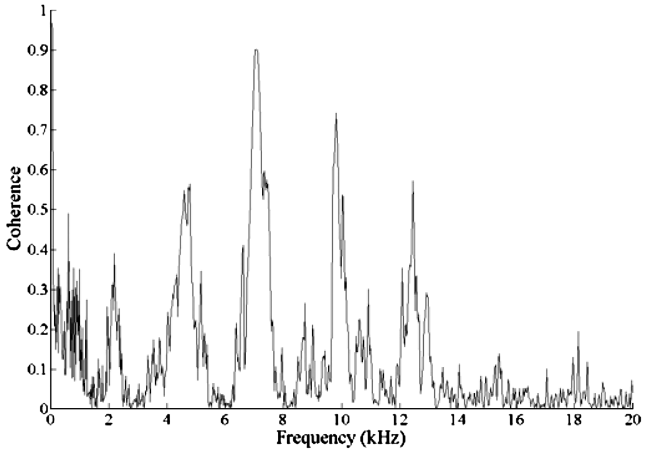

Fig. 20 Coherence between front- and aft-wall pressure signals for the cavity with a ramp angle of 45 deg.

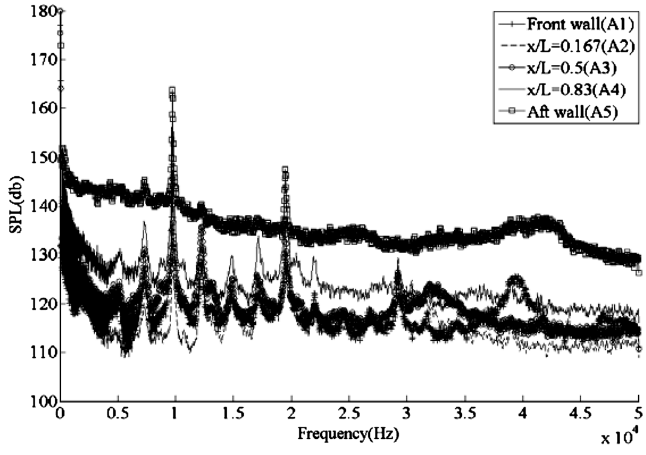

Fig. 21 SPL at different locations inside the cavity with a ramp angle of 30 deg.

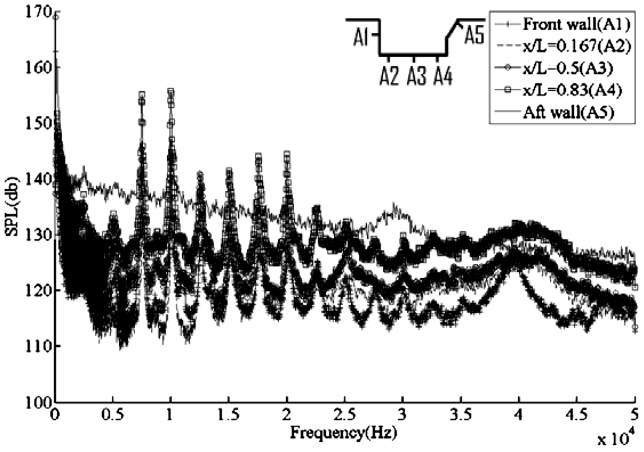

Fig. 22 SPL at different locations inside the cavity with a ramp angle of 15 deg.

that four distinct modes exist; the magnitude of the modes resembles that of the cavity with a ramp angle greater than 45 deg. At higher frequencies, the spectrum is broadband with no distinct peaks for both the cavities. On examining the spectra of other locations in both figures, it is noted that the peaks exist at frequencies ranging from lower to higher values, although the magnitudes are smaller in the cavity with a ramp angle of 30 deg compared with that of 15 deg. These include modes at frequencies corresponding to those frequencies at which modes exist in the spectra of the aft-wall signal pressure signal. This means that for locations inside the cavity there exist modes at frequencies where modes do not exist in the spectra of the aft wall. This shows that the phenomenon causing additional modes to exist inside the cavity has no influence on the spectra of the aft wall. This behavior was not observed in cavities with higher ramp angles and could be due to the periodic movement of vortices or waves that are still to be understood inside the cavity.

A similar study was performed by the authors on cavities having different aft-wall slopes and a length/depth ratio of 3. The schematic of such a cavity is shown in Fig. 23. The effective lengths of these cavities are exactly the same as those of the cavities under present study. The spectra of the cavities with an aft-wall angle of 30 and 15 deg, respectively, are shown below. It is worthwhile if these are compared with the present results on 30 and 15 deg ramp-angle cavities.

The locations of transducers A1, A2, A3, and A4 shown in Fig. 24 match with the locations A1, A2, A3, and A5, respectively, in Fig. 21. Similarly, transducers A1, A2, and A4 in Fig. 25 match with the locations A1, A2, and A5, respectively, in Fig. 22. Considering locations A4 in Fig. 24 and A5 in Fig. 21, it is noted that high-amplitude modes exist at these locations. The instantaneous shadowgraph images show that the reflected shock from the ceiling of the test section impinges at this transducer location. It is justifiable to conclude that the high-amplitude tones at these locations are due to the impingement of reflected shock. On other transducer locations in both cavities, if the reflected shock were the only source of influence, the amplitude of oscillations at the aforementioned locations should have been more or less the same. A major disparity in behavior of the spectra between Figs. 21 and 24 and between Figs. 22 and 25 has been noted. This indicates that the oscillations in Figs. 21 and 22 are due to the cavity flowfield, independent of the wave reflections.

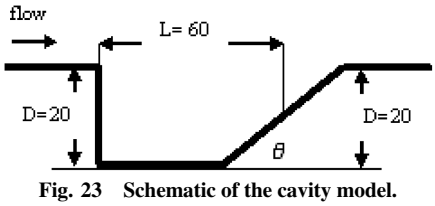

Fig. 23 Schematic of the cavity model.

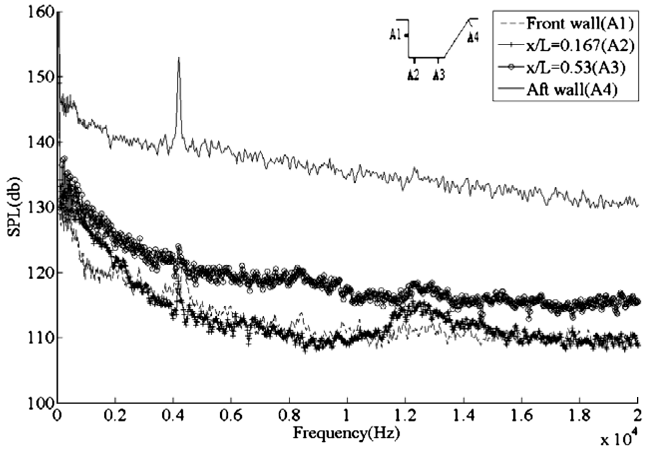

Fig. 24 SPL at different locations inside the cavity with an aft-wall angle of 30 deg.

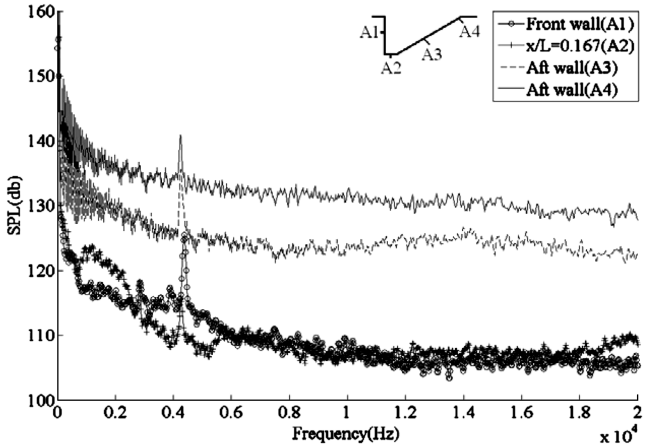

Fig. 25 SPL at different locations inside the cavity with an aft-wall angle of 15 deg.

Referring back to the cavity with a 30 deg ramp angle, Fig. 26 shows normalized cross correlation between the aft-wall pressure signal and pressure signals from other locations inside the cavity plotted for the entire time duration for which signals were acquired. It is noted that there exists positive correlation at all locations and the aft wall, except between $x/L = 0.167$ and the aft wall between time lags 0 and 0.1 s. Maximum positive cross correlation between pressure signals at the front and aft walls is 0.15, occurring at time 0.30 s. This shows that the disturbance takes longer time to reach the front wall, which indicates that unlike in higher-aft-wall-angled cavities, this disturbance is not an upstream-traveling acoustic wave.

Figure 27 shows normalized cross correlation between the aft-wall pressure signal and pressure signals from other locations inside the cavity plotted for the entire time duration for which signals were acquired. On examining the autocorrelation, it is noted that the oscillations have dampened considerably with time. On observing the cross correlation at different locations except at $x/L = 0.83$, it is observed that at zero time delay the coefficients have large negative value. Maximum positive cross correlation between pressure signals at the front and aft walls is 0.27, occurring at time 0.35 s. Similar to the 30 deg ramp-angle cavity, this is indicative of the absence of an upstream-traveling acoustic wave.

Coherence between the front-wall and aft-wall pressure signals is shown in Figs. 28 and 29 for cavities with a ramp angle of 30 and 15 deg, respectively. It is seen that a high-to-moderate value of coherence occurs at frequencies at which modes exist in the spectra of the aft wall. For other frequencies the value of coherence is very small. This means that although there exist modes at different frequencies in the spectra of the front wall, the value of coherence at these frequencies is small. It has high value at those frequencies where modes exist in the spectra of aft wall. This further substantiates that the phenomenon influencing additional modes to exist inside the cavity has no effect on the aft-wall location, as stated earlier in conjunction with Figs. 21 and 22.

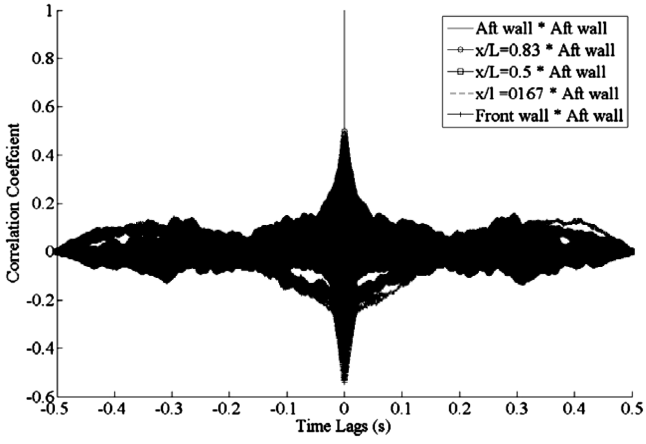

Fig. 26 Normalized cross correlation of pressure signals for the cavity with a ramp angle of 30 deg.

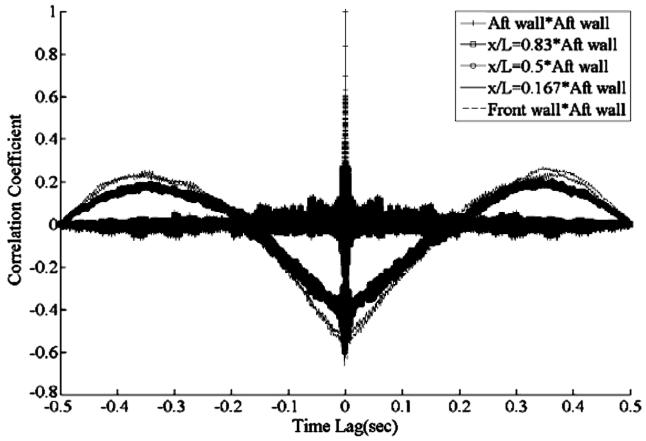

Fig. 27 Normalized cross correlation of pressure signals for the cavity with a ramp angle of 15 deg.

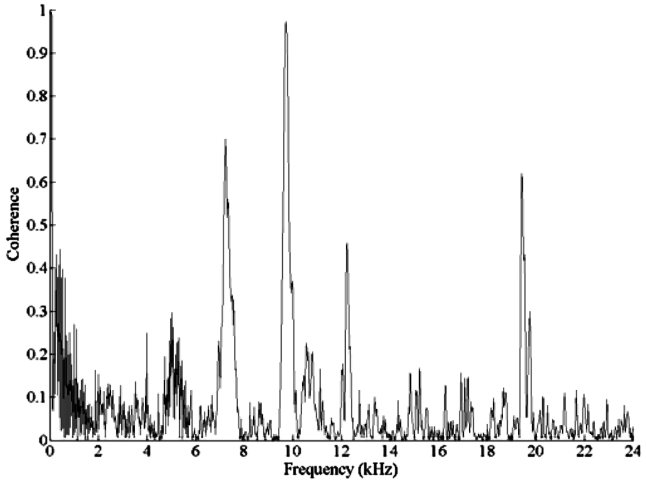

Fig. 28 Coherence between front- and aft-wall pressure signals for the cavity with a ramp angle of 30 deg.

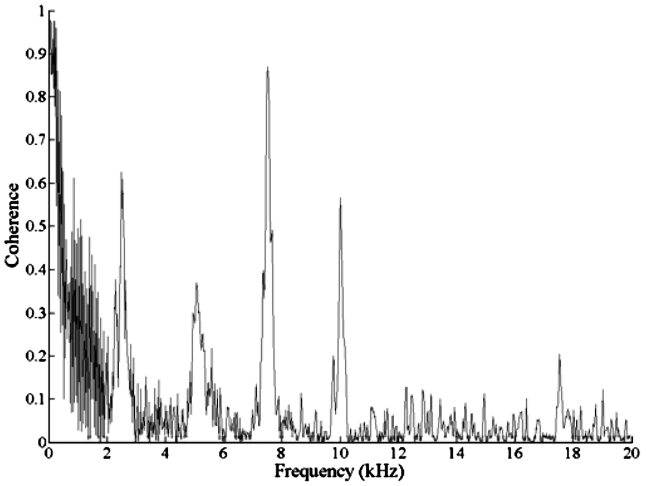

Fig. 29 Coherence between front- and aft-wall pressure signals for the cavity with a ramp angle of 15 deg.

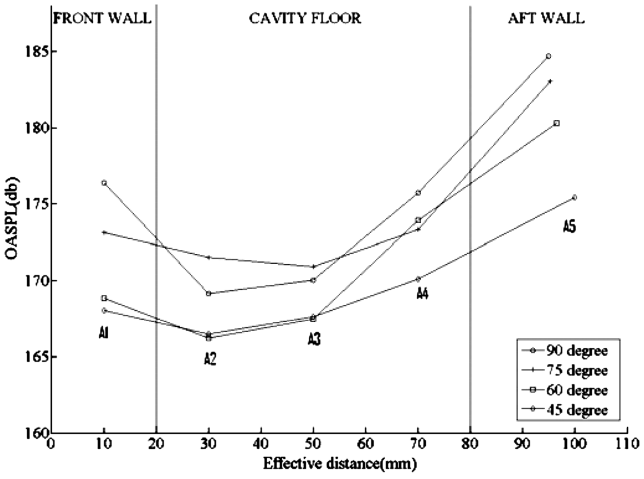

Fig. 31 OASPL of cavities with different ramp angles at different locations inside the cavity: a) front wall, b) $x/L = 0.163$, c) $x/L = 0.5$, and d) $x/L = 0.83$.

6. Comparative Study

Cavities with different ramp angles were compared at a few locations, as shown in Fig. 30. On examining the plots, it is seen that at a particular location, the dominant mode shifts to a higher frequency as the ramp angle is reduced. It is observed that the cavity with a ramp angle of 45 deg produces lower oscillations in comparison with all the other cavity configurations considered. Perng and Dolling [17] carried out a similar experiment at Mach 5 using cavities with 90, 59.8, 51.3, and 45 deg ramp angles. The present result, that the cavity with a 45 deg ramp produces the lowest oscillations, agrees with that in [17].

It is observed that as the ramp angle decreases, the cavity oscillations dampen up to 45 deg; with further reduction in ramp angle, the oscillations increase. All of the above observations were noted irrespective of location within the cavity. It is further found that for cavities with ramp angles of 30 and 15 deg, the modes exist even at higher frequencies, which is not the case with cavities with higher ramp angles.

The change in broadband spectrum can be understood better by plotting the overall sound pressure level (OASPL) [where $\mathrm{OASPL} = 20\ \log(P_{\mathrm{rms}}/20\ \mu\mathrm{Pa})$], which represents the total energy under the spectra.

Figure 31 shows the OASPL of cavities with different ramp angles at different locations inside the cavity. It is seen that the highest OASPL occurs at the aft-wall location for the cavities under consideration. This is due to direct impingement of the shear layer. As the ramp angle is lowered, the OASPL decreases due to a change in the impingement angle of the shear layer. Considering the front

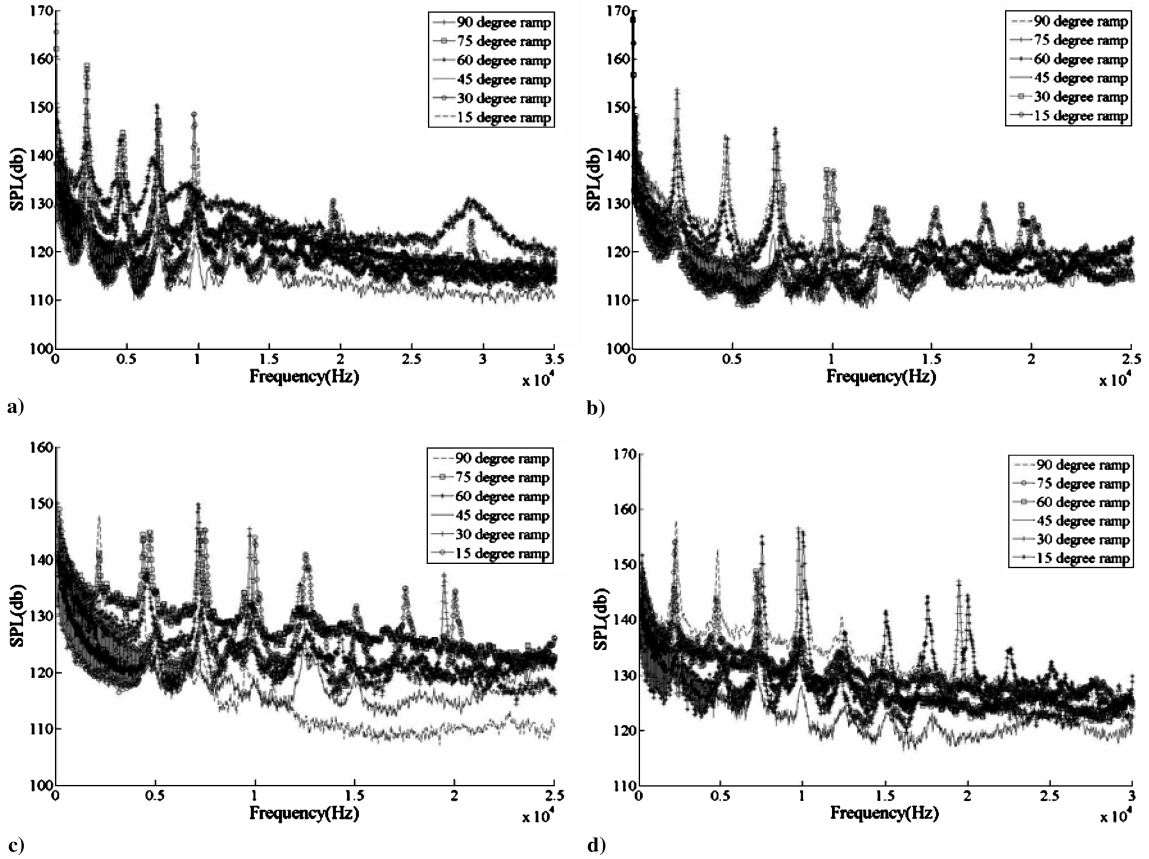

Fig. 30 SPL of cavities with different ramp angles at different locations inside the cavity: a) front wall, b) $x/L = 0.163$, c) $x/L = 0.5$, and d) $x/L = 0.83$.

wall, it is observed that as the ramp angle reduces, the OASPL decreases. This is due to the fact that as the ramp angle is reduced, the strength of the acoustic wave is reduced. On the floor of the cavity, the highest OASPL occurs at $x/L = 0.83$ compared with the other locations. Almost certainly, the reason for this is that the turbulent shear layer and freestream fluid enters into the cavity at the trailing edge. The lowest value occurs on the cavity floor near the front wall. In general, it is noted that the baseline cavity has the highest OASPL, whereas the cavity with a ramp angle of 45 deg has the lowest at all locations. This is in agreement with the results of the computational study of Soemarwoto and Kok [22] on supersonic flow over rectangular and 45 deg ramp-angle cavities. For all cavities, the highest OASPL occurs at the aft-wall location and the lowest occurs at $x/L = 0.163$.

IV. Conclusions

Supersonic flow over cavities with different ramp angles of 75, 60, 45, 30, and 15 deg is studied experimentally. The study includes flow visualization and unsteady pressure measurements. Instantaneous shadowgraph images indicate the presence of four different types of waves in the case of cavities with ramp angles of 90–60 deg. The shear layer is predominantly wavy in nature, suggesting that these cavities generate strong oscillations. In the case of cavities with ramp angles of 45–15 deg, only the leading-edge wave could be observed. The shear layer is found to be less wavy in contrast to their higher-angled counterparts. Analysis of the spectra of unsteady pressure signals shows that there is marginal drop in SPL as the ramp angle is decreased from 90 to 60 deg. This is possibly due to the decrease in strength of the acoustic wave as the ramp angle decreases. A steep fall in amplitudes of oscillations is observed in the case of the cavity with a ramp angle of 45 deg. Irrespective of the ramp angle, high-amplitude oscillations as well as broadband noise occur at the aft wall, presumably due to the direct impingement of the shear layer. As the ramp angle is reduced, dominant modes shift toward higher frequency. Temporal mode switching is seen to be clearly influenced by the change in ramp angle for higher-angled cavities. As the angle is reduced, multiple modes coexist, signifying that switching between the modes is decreased. Cross-correlation plots indicate the presence of an upstream-traveling acoustic wave inside the cavity for cavities with ramp angles between 90 and 60 deg, whereas for the cavity with a ramp angle of 45 deg, the presence of an acoustic wave is not discernible. The sharp drop in amplitudes of oscillations for the cavity with a ramp angle of 45 deg is attributed to the absence of acoustic wave, as confirmed from the correlation plots. A spectral plot of the cavities with ramp angles of 30 and 15 deg shows an increase in amplitude of oscillations at locations inside the cavity, whereas the cross-correlation plots indicate the absence of an upstream-traveling wave. The reasons for this behavior are still to be understood. Plots of coherence indicate good interdependence between the phenomena occurring at the front and aft walls for cavities with higher ramp angles. The dependence decreases as the angle of the ramp decreases. The overall behavior of the baseline cavity and cavities with 75 and 60 deg ramp angles is similar.

References

[1] Krishnamurthy, K., "Acoustic Radiation from Two-Dimensional Rectangular Cutouts in Aerodynamic Surface," NASA TN-3487, 1955.

[2] Rossiter, J. E., "Wind Tunnel Experiments on the Flow over Rectangular Cavities at Subsonic and Transonic Speeds," Aeronautical Research Council, Reports and Memoranda No. 3438, 1964.

[3] Heller, H. H., Holmes, D. G., and Covert, E. E., "Flow-Induced Pressure Oscillations in Shallow Cavities," *Journal of Sound and Vibration*, Vol. 18, No. 4, 1971, pp. 545–553. doi:10.1016/0022-460X(71)90105-2

[4] Rockwell, D., and Naudascher, E., "Review: Self-Sustaining Oscillations of Flow Past Cavities," *Journal of Fluids Engineering*, Vol. 100, No. 2, 1978, pp. 152–165.

[5] Zhang, X., and Edwards, J. A., "An Investigation of Supersonic Oscillatory Cavity Flows Driven by Thick Shear Layers," *The Aeronautical Journal*, Vol. 94, No. 940, 1990, pp. 355–364.

[6] Vakili, A. D., and Guthier, C., "Control of Cavity Flow by Upstream Mass Injection," *Journal of Aircraft*, Vol. 31, No. 1, Jan.–Feb. 1994, pp. 169–174. doi:10.2514/3.46470

[7] Cattafesta, L. N., Shukla, D., Garg, S., and Ross, J. A., "Development of an Adaptive Weapons-Bay Suppression System," AIAA Paper 99-1901, May 1999.

[8] Zhuang, N., Alvi, F. S., Alkislar, M. B., and Shih, C., "Supersonic Cavity Flows and Their Control," *AIAA Journal*, Vol. 44, No. 9, 2006, 2118–2128.

[9] Ukeiley, L. S., Ponton, M. K., Seiner, J. S., and Jansen, B., "Suppression of Pressure Loads in Cavity Flows," AIAA Paper 2002-0661, Jan. 2002.

[10] Stanek, M. J., Raman, G., Ross, J. A., Odedra, J., Peto, J., Alvi, F., and Kibens, V., "High Frequency Acoustic Suppression—The Mystery of Rod-in-Crossflow Revealed," AIAA Paper 2003-0007, Jan. 2003.

[11] Bueno, P. C., Ünalmis, Ö. H., Clemens, N. T., and Dolling, D. S., "The Effect of Upstream Mass Injection on a Mach 2 Cavity Flow," AIAA Paper 2002-0663, Jan. 2002.

[12] Sarno, R. L., and Franke, M. E., "Suppression of Flow-Induced Pressure Oscillations in Cavities," *Journal of Aircraft*, Vol. 31, No. 1, 1994, pp. 90–96. doi:10.2514/3.46459

[13] Sarohia, V., and Massier, P. F., "Control of Cavity Noise," *Journal of Aircraft*, Vol. 14, No. 9, 1977, pp. 833–837. doi:10.2514/3.58862

[14] Sahoo, D., Annaswamy, A. M., Zhuang, N., and Alvi, F., "Control of Cavity Tones in Supersonic Flow," AIAA Paper 2005-0793, Jan. 2005.

[15] Zhang, X., Rona, A., and Edwards, J. A., "The effect of Trailing Edge Geometry on Cavity Flow Oscillation Driven by a Supersonic Shear Layer," *The Aeronautical Journal*, Vol. 102, No. 1013, March 1998, pp. 129–136.

[16] Kuo, C.-H., and Huang, S. H., "Influence of Flowpath Modification on Oscillation of Cavity Shear Layer," *Experiments in Fluids*, Vol. 31, No. 2, 2001, pp. 162–178. doi:10.1007/s003480100270

[17] Perng, S. W., and Dolling, D. S., "Suppression of Pressure Oscillations in High Mach Number, Turbulent, Cavity Flow," *Journal of Aircraft*, Vol. 38, No. 2, 2001, pp. 248–256. doi:10.2514/2.2782

[18] Gruber, M. R., Baurle, R. A., Mathur, T., and Hsu, K. Y., "Fundamental Studies of Cavity-Based Flame Holder Concepts for Supersonic Combustors," *Journal of Propulsion and Power*, Vol. 17, No. 1, 2001, pp. 146–154. doi:10.2514/2.5720

[19] Sun, M. B., Liang, J. H., and Wang, Z. G., "Numerical Study on Self-Sustained Oscillation Characteristics of Cavity Flameholders in a Supersonic Flow," *Journal of Aerospace Engineering*, Vol. 222, No. ??, 2008, pp. 95–102.

[20] Bauer, R., and Dix, R., "Engineering Model of Unsteady Flow in a Cavity," Arnold Engineering Development Center, TR AEDC-TR-91-17, Arnold AFB, TN, Dec. 1991.

[21] Clarke, R. L., Kaufman, L. G., and Maciulaitis, A., "Aeroacoustic Measurements for Mach 0.6–3.0 Flows Past Rectangular Cavities," AIAA Paper 80-0036, 1980.

[22] Soemarwoto, B. I., and Kok, J. C., "Computations of Three-Dimensional Unsteady Supersonic Cavity Flow to Study the Effect of Different Downstream Geometries," National Aerospace Lab. (NLR), Rept. NLR-TP-2001-446, Amsterdam, 2001.

T. Jackson
Associate Editor